Assessing Parameterized Geometric Models of Woven Composites using Image-Based Simulations

Collin Foster

Overview

Mesoscale simulations of woven composites using parameterized geometries offer a way to connect constituent material properties and their geometric arrangement to effective composite properties. However, the reality of as-manufactured materials often differs from the ideal, both in terms of tow geometry and manufacturing heterogeneity. We employ mesoscale finite element method simulations to compare idealized analytical and as-manufactured woven composite materials and study the sensitivity of their effective properties to the mesoscale geometry. Image geometries are reconstructed from X-ray computed tomography; image segmentation is performed using deep learning methods. The result of this work is that an analytical geometry can be used to reasonably predict the effective thermal properties of a multi-layer production composite.

Introduction

Construction of analytical composite weaves enables convenient rapid design studies to evaluate thermal protection systems (TPS) when the material is not readily available. Weave generators are useful tools for idealized or dry weaves, but the generation of symmetric cross-sectional geometry often misrepresents as-manufactured cured weaves. Alternatively, tomographic data of as-manufactured materials enables direct numerical predictions of the TPS technologies. Being able to perform simulations directly on composite geometries allows for valuable structure-property relations and performance estimates without expensive testing and characterization, greatly reducing the time required for design and optimization. High resolution X-ray computed tomography (XCT) is a non-destructive technique with sub-micron resolution capability that is currently used to evaluate complicated 3D woven composites of various compositions at multiple length scales. Regions of interest are resolved with XCT that can then be matched with relevant experimental property data to infer predictions on scaled systems of similar materials. This study examines how well a single-layer (SL) XCT is represented by an analytical geometry over relevant thermal and topological properties. Initially, we investigate whether an image-based SL woven TPS can approximate a larger, multi-layer coupon specimen of similar weave architecture.

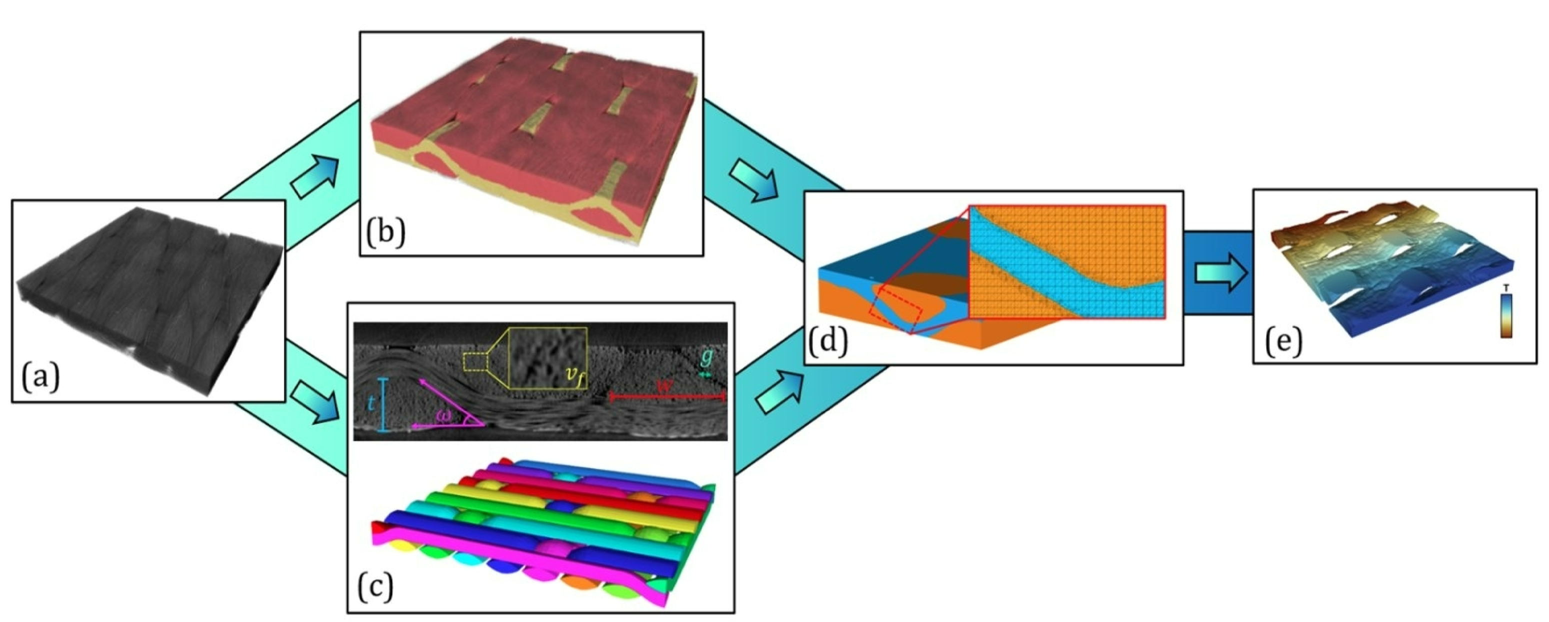

Figure 1. Workflow for analytical and image-based TPS simulations illustrated for a single-layer composite. (a) 3D reconstruction of the raw m-CT image. (b) Three-phase image segmentation. (c) Analytical geometry informed by parameter extracted from the XCT image. (d) Volume mesh. (e) Physics simulation result.

Method and Setup

The reconstruction of the SL image geometry is captured as the raw XCT dataset without segmentation. We utilize a U-Net [1] deep convolutional neural network implemented in Dragonfly to segment the warp from the weft tows. Each dataset is first surface then volumetrically meshed using the Conformal Decomposition Finite Element Method [2]. Effective thermophysical properties of the composite are calculated using finite element simulations performed by the Sandia-developed code Sierra/Aria [3]. Analytical and image-based geometries are evaluated for fiber volume fraction, specific surface area, specific contact area, density, specific heat, IP and OOP conductivity.

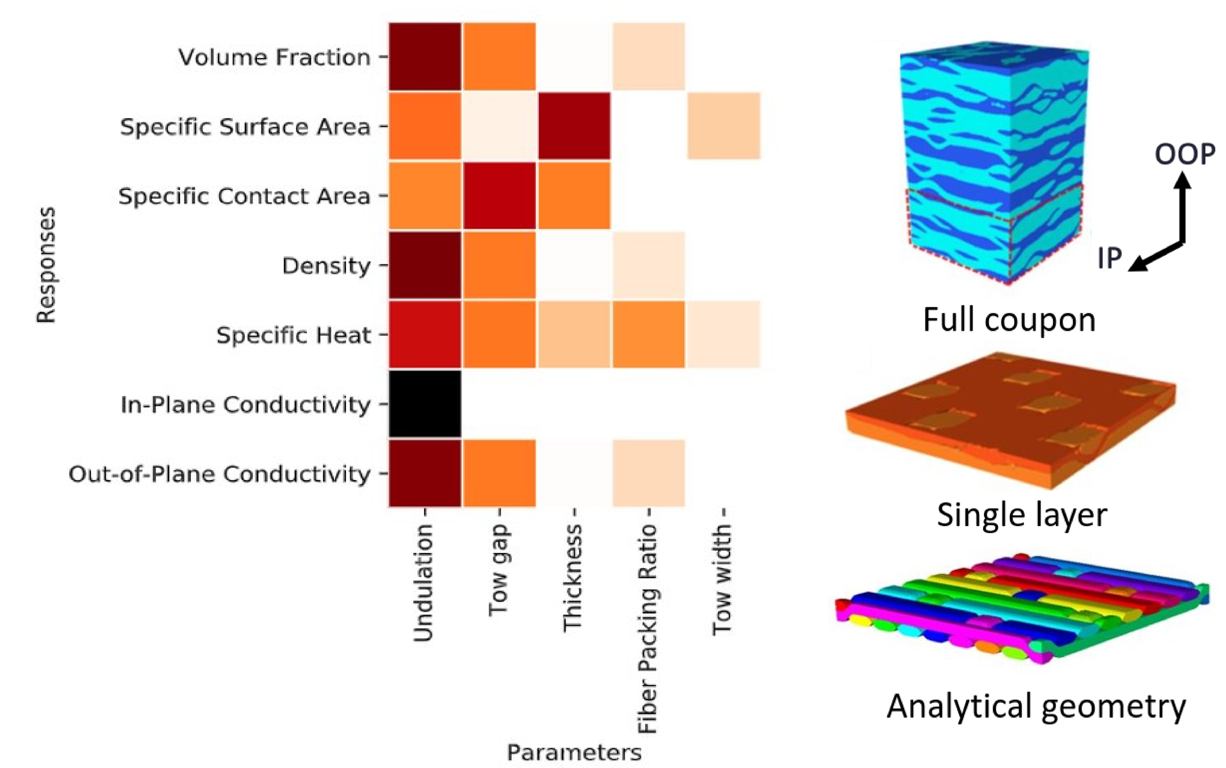

Figure 2. Analytical geometry's influence on effective properties. Analytical tow-shape and curvature determined from measurements on real single-layer XCT.

Results

Depicted in Fig. 2, undulation plays largely in determining the shape of the tow, and as such, has clear influence on all properties dependent on the shape: volume fraction, density, specific heat, in- and out-of-plane conductivities. The tow gap describes the space between neighboring tows measured from the SL image geometry. Many of the tow gaps sampled are nearly zero in length, increasing the relative amount of heat conducted through the weave and allowing a more connected pathway for thermal transport. Again, for the in-plane direction, tows aligned with the thermal gradient dominate the thermal transport and perpendicular tows, or the resin matrix, have relatively little importance. Tow thickness and width do not show significant influence on thermal properties through the Sobol' indices. Instead, they come through on properties more dependent on the resin such as specific heat. Shown in Fig. 3 are the representative image-based SL and coupon results compared to those from the analytical study. IP conductivity for the image geometries is in good agreement with SL analytical geometries having a high fiber volume fraction. Because of the increased axial tow conductivity simulated, there is a strong correlation between the volume fraction and IP conductivity for the analytical geometries. The OOP conductivities for the image geometries are slightly lower when compared to the SL analytical geometry.

At high volume fractions in which the image and analytical geometries are similar, the analytical SL has a very low undulation (square-wave) tow movement. The analytical tows moving OOP are very direct routes for thermal transport between the two prescribed thermal boundary conditions, this also accounts for the non-constant variation of analytical OOP thermal conductivity as volume fraction increases. Additionally, because of its highly compact nature from manufacturing, it is possible much of the undulation observed has been suppressed in the image-based geometries. As the Sobol' indices (Fig. 2) have shown, an overestimate of tow undulation will have a large influence on, and a drastic reduction in, OOP thermal conductivity. Quantities such as density and specific heat are not dependent on the geometry directly, but on the relative amounts of each phase in the unit cell. Therefore, both are linear with respect to fiber volume fraction.

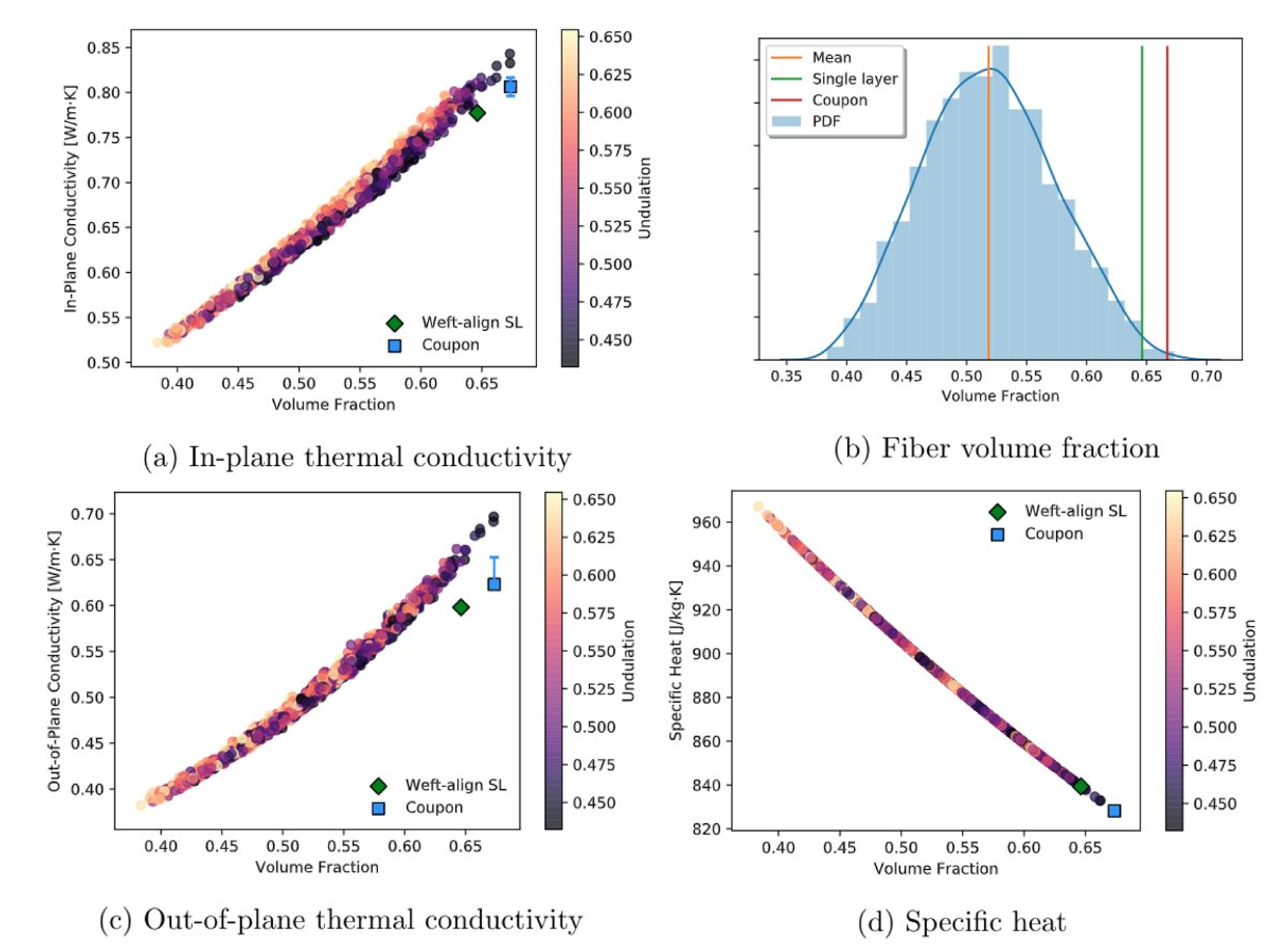

Figure 3. Effective property results from the analytical geometry study (scatter) compared to image-based simulations. (a) In-plane thermal conductivity, (b) fiber volume fraction, (c) out-of-plane thermal conductivity, and (d) specific heat.

Conclusions

For the composite samples scanned and simulated in this study, the corresponding analytical geometries can represent the image-based geometry with select caveats. Due to the high compaction, layer nesting, and weave deformation seen in the imperfect manufactured samples, the synthetic geometries are not able to fully achieve comparable fiber volume fractions, even when using parameters measured from the XCT data. However, at low undulation values, where the fabric is highly crimped and the space between tows is reduced, the analytical geometries can obtain representative fiber volume fractions. With these combinations of parameters, the analytical geometries produce comparable results for thermal conductivity in the IP direction, as well as specific heat. Out-of-plane conductivity is not as promising, due to the very low undulation that comes with the analytical SL achieving comparable volume fraction to the image-based geometries.

Contact

Collin Foster, PhD Candidate
Center for Hypersonics and Entry Systems Studies
Department of Mechanical Science and Engineering
University of Illinois at Urbana-Champaign
Email: collinf3@illinois.edu
Website: chess.grainger.illinois.edu

Acknowledgements

Sandia National Laboratories is a multimission laboratory managed and operated by National Technology & Engineering Solutions of Sandia, LLC, a wholly owned subsidiary of Honeywell International Inc., for the U.S. Department of Energy's National Nuclear Security Administration under contract DE-NA0003525.
U.S. Department of Education's Graduate Assistance in Areas of National Need Fellowship Program award P200A180050-19.
U.S. Department of Energy's Office of Science Graduate Student Research (SCGSR) Program.

References

1. O. Ronneberger, P.Fischer, and T. Brox, (2015) 234-241
2. D. R. Noble, E. P. Newrn, and J. B. Lechman, (2010) *International Journal for Numerical Methods in Fluids* 63.6, 725-742
3. SIERRA Multimechanics Module: Aria User Manual - Version 4.56